

The Limits of Signal Averaging in Atmospheric Trace-Gas Monitoring by Tunable Diode-Laser Absorption Spectroscopy (TDLAS)

P. Werle, R. Mücke, F. Slemr

Fraunhofer Institute for Atmospheric Environmental Research, Kreuzackbahnstrasse 19, D-82453 Garmisch-Partenkirchen, Germany
(Fax: +49-8821 /73573 E-Mail : PWWerle@aol.com)

Received 12 February 1993/Accepted 20 April 1993

Abstract. Modern research in atmospheric chemistry requires highly sensitive techniques for the measurement of concentrations of free radicals which determine the rate of photochemical destruction of most atmospheric pollutants. Tunable diode-laser absorption spectroscopy (TDLAS) has already been successfully used for measurements of very low concentrations of stable gases, but further improvement in its sensitivity by signal averaging has been limited by the stability of the instrument. In this paper the concept of the Allan variance is utilized to analyze the stability of an existing frequency-modulated (FM) TDLAS instrument leading to a detection limit for NO₂ of 34 pptv at 6 Hz detection bandwidth. The stability of the instrument allows averaging over 60 s. Taking into account the measuring cycle consisting of the determination of the sample spectra and zero air spectra as well as gas exchange in the absorption cell, the detection limit achievable with this particular instrument was 10 pptv within 25 s under laboratory conditions. Possibilities of further improvement of the detection limit are discussed.

PACS: 07.65

Tunable diode laser absorption spectroscopy (TDLAS) is being frequently used for measurement of trace gas pollutants in the atmosphere [1]. The TDLAS spectrometers usually work with multipass absorption cells to achieve high sensitivity. To alleviate problems by absorption line overlap, these absorption cells are usually operated at low pressure where the linewidth is Doppler limited. In most sensitive instruments the diode laser is repetitively tuned over an absorption line of a target molecule and the absorption spectra are averaged over a specified time interval. Additional modulation techniques are used to reduce the 1/f laser noise. With wavelength modulation, typically, detection limits¹ of

¹ Throughout this paper we use as a definition of detection limit the standard deviation derived from the variance of the mean to be comparable with the Allan variance. For practical measurements the definition of the International Organisation for Standardization (ISO/DIS 9169) is recommended, where the determination of performance characteristics of measurement methods for air quality is specified

the order of 0.1 ppbv (1 ppbv = 10⁻⁹ volume mixing ratio) were achieved for many smaller molecules in the air with spectra averaging time of a few minutes [2-5]. Although these detection limits are sufficient for many applications, still better detection limits are required by modern atmospheric research for the determination of concentrations of free radicals which play a decisive role in the destruction of almost all atmospheric pollutants and in the formation of tropospheric ozone [2, 6, 7]. The required detection limits are of the order of a few pptv (1 pptv = 10⁻¹² volume mixing ratio for HO₂ and even lower for HO radicals [7].

Substantial improvements of TDLAS detection limits were obtained by introducing high-frequency modulation techniques [8-11]. In terms of optical density the best detection limits obtained so far with a high-frequency modulated TDLAS instrument with a multiple-pass absorption cell were of the order of 10⁻⁷ with a detection bandwidth of 1 Hz [11]. At these sensitivities interference fringes due to unwanted etalons are becoming the factor limiting further improvement of the detection limits [11]. To achieve the aforementioned detectable optical density, several techniques to reduce the magnitude of these fringes had to be applied, such as dithered Brewster-angle plate [12] or mirror [13], low-frequency jitter of the laser current [14], and low-pass filtering [15]. A substantial further improvement of the TDLAS sensitivity by these and similar techniques or their combination is hard to achieve [11].

In principle, the problem of fringe limitation can be solved by subtraction of a zero air spectrum from the measured spectrum. Trace-gas measurements near to the detection limit are, therefore, usually performed by measuring alternatively the spectrum of the ambient air and the spectrum of zero air, i.e. air devoid of the target substance [16]. This procedure is based on the inherent assumption that within the time interval needed for the acquisition of both the measurement and the background spectra the fringes do not move. If this assumption is fulfilled, the subtraction of the background spectrum from the measurement spectrum would provide the absorption spectrum of the target species which, to a first approximation, is only subject to random noise. Further averaging of these corrected spectra should then improve the

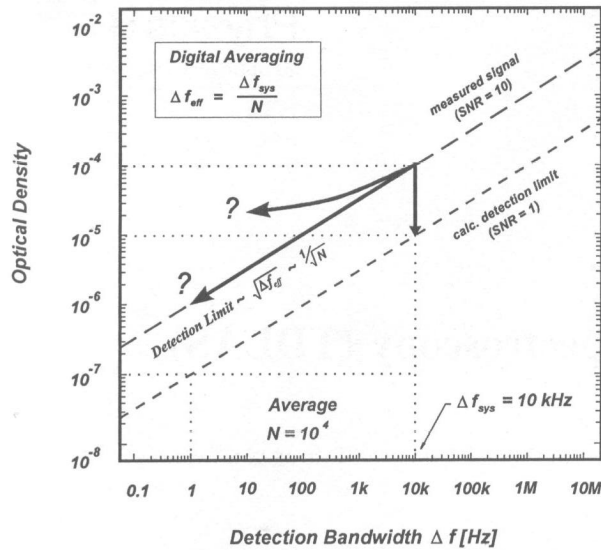


Fig. 1. Determination of the detection limit. What is the result of digital averaging of 10^4 spectra and which curve does the detection limit follow? How long does the relationship $\Delta f_{eff} = \Delta f_{sys}/N$ hold?

detection limit according to a square-root relationship [9]. This behavior is illustrated in Fig. 1. Let us assume a TD-LAS spectrometer capable of detecting an optical density of 10^{-4} at the system detection bandwidth of $\Delta f_{sys} = 10$ kHz with a signal-to-noise ratio (SNR) of 10; this corresponds to a detection limit (with SNR = 1) of 10^{-5} at 10 kHz. By averaging 10^4 spectra, the effective bandwidth of the instrument will be reduced to 1 Hz and this reduction should result in a detection limit of 10^{-7} at SNR = 1. This has been tried several times (e.g. [17, 18]) but the achieved improvement was always substantially smaller than that expected one on the basis of the square-root relationship. The observed deviations are most probably caused by the violation of the above assumption and, consequently, the stability of the TDLAS instrument has to be investigated.

The stability of a TDLAS instrument is analyzed in this paper in terms of the ‘‘Allan variance’’. In the first section, the concept of the ‘‘Allan variance’’ is introduced as a tool to characterize the stability of any TDLAS instrument. The utility of this tool is discussed in the second section. In the third section, the performance of a real frequency modulated TDLAS instrument is analyzed in terms of ‘‘Allan variance’’ and several sources for instrument drift will be identified and discussed. The stability of the instrument allows averaging over 60 s. Taking into account the measuring cycle consisting of the determination of measurement and zero air spectra as well as gas exchange in the absorption cell, the ultimate sensitivity achievable with this particular instrument was 10 pptv with a measurement time of 25 s.

1 Allan Variance and Variance of the Mean

Practical measurements usually consist of a sequence of sample and background measurements. After digital background subtraction and some additional filtering the resulting spectrum is fitted to a stored calibration spectrum using a regression algorithm, which calculates concentration values and

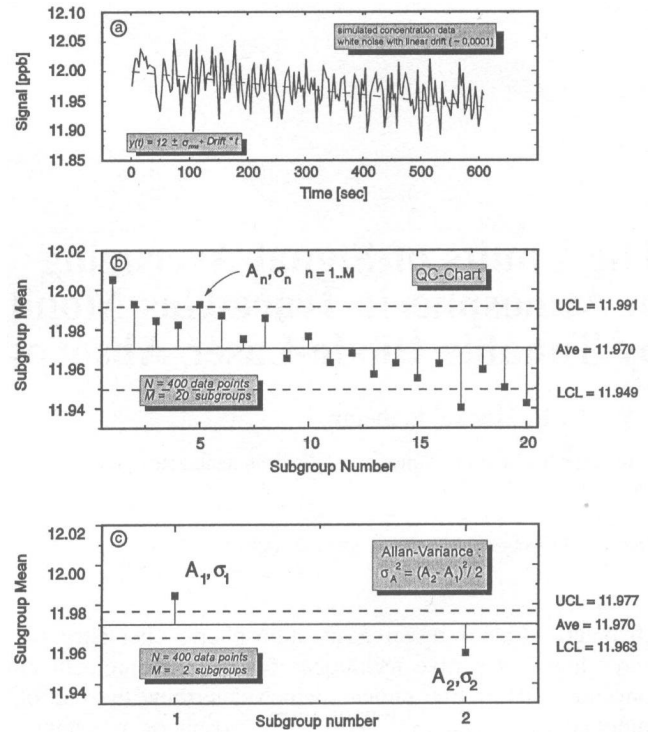


Fig. 2. a Simulated concentration time series data containing white noise and a linear negative drift; b QC-chart of data from a with calculated upper (UCL) and lower (LCL) confidence levels; c QC-chart where a special choice of $M = 2$ was made

the associated errors. We noted that the detection limit and the confidence range depend strongly on the quality of input data, especially on the variance of the measured data. In most spectroscopic applications the output data are mean values from an averaging process and therefore the variance of this mean has to be used for the calculation of the detection limit. It is obvious that any improvement of the detection limit depends strongly on the stability of the system.

In order to analyze the stability, some typical quantities to investigate might be the laser intensity, the line center position of a measured signal, the laser temperature and current, or calculated concentration values from a calibration setup. For a formal description of the stability of our spectrometer we assume a recorded set of N time-series data referring to amplitude or frequency stability represented by $x_i, i = 1 \dots, N$, with N of the order of 10^3 - 10^4 . For modeling purposes such a data set can be generated using the equation $x_i = a + bi + G(a)$, where a is a DC offset, and b is the coefficient for a linear drift. Such a data set x_i , containing Gaussian distributed white noise $G(a)$ with a small linear drift component superimposed, is shown in Fig. 2a. This data set can be described by its average value A and the variance σ^2 , which are defined by :

$$A = \frac{1}{N} \sum_{i=1}^N x_i, \quad \sigma^2 = \frac{1}{N-1} \sum_{i=1}^N (x_i - A)^2, \quad (1)$$

and a variance of the mean $\text{Var}(A) = \sigma^2/N$. In general, the N elements of the original data set can be divided into M subsets containing k elements where $M = N/k$. For each of these M subgroups an average value A , and a variance

σ_n^2 can be calculated:

$$A = \frac{1}{k} \sum_{l=1}^k x_{(n-1)k+l}, \quad (2)$$

$$\sigma_n^2 = \frac{1}{k-1} \sum_{l=1}^k (x_{(n-1)k+l} - A_n)^2,$$

and the variance of the mean is defined by $\text{Var}(A_n) = \sigma_n^2/k$ where n denotes the subgroup number and k is the number of elements in the subgroup n . A plot generated from these subgroup averages is shown in Fig. 2b; it is used for quality control purposes (QC-Chart) [19,20]. In these charts the calculated arithmetic sample average is plotted together with an upper and a lower confidence limit (UCL/LCL). The subgroup averages, which are included in the plot, show a significant drift in the analyzed time series data. The question whether two subsequent averages can be further averaged is answered using statistical tests (F-test, t-test) [21,22]. The analysis of a long dataset can be very time consuming and, therefore, it would be convenient to find a more efficient method to determine the optimum averaging group size. Based on the definition of the general variance [23]

$$\sigma^2(M, T, \tau) = \frac{1}{M-1} \sum_{n=1}^M (A_n - A)^2, \quad (3)$$

where M is the number of groups used in obtaining a sample variance, T is the time interval between the beginning of two successive measurements and τ is the integration time. To investigate the variance of the mean A , which is defined by:

$$\text{Var}(A) = \sigma^2/N = \sigma^2 / Mk, \quad (4)$$

no special assumptions will be made. Equation (4) can be used with a special choice for the number of subgroups M ; for convenience, if we choose $M = 2$ the number of elements in each subgroup $k = N/2$ (Fig. 2c). This yields the following expression for the variance of the mean:

$$\text{Var}(A, M = 2) = \frac{1}{2-1} \sum_{n=1}^2 (A_n - A)^2$$

$$= \frac{1}{2} [A_2 - A_1]^2 \equiv \sigma_A^2 = \sigma^2 / (2k). \quad (5)$$

σ_A^2 is the well known ‘‘Allan-Variance’’, which was introduced by Allan [24] in 1966 for the characterization of frequency standards (see next section). It can be shown that the choice of $M = 2$ is the best value for high drift sensitivity [23]. The so called ‘‘bias function’’, B_1 , defined by:

$$B_1(M, r, \mu) \equiv \frac{\langle \sigma^2(M, T, \tau) \rangle}{\langle \sigma^2(2, T, \tau) \rangle}, \quad (6)$$

is tabulated in [25] and reflects the ratio between the general variance and the Allan variance for a given ratio $\tau = T/\tau$ and a given noise type μ . For white noise (represented by $\mu = -1$), the bias function $B_1 = 1$. This is very important, because it means that, in the case of a white-noise dominated system, the Allan variance is equivalent to the variance of the mean and, as the variance of the mean is a measure for the detection limit, the Allan variance can be used to predict the detection limit.

Until now only a single value for the Allan variance has been calculated. For an instrument characterization the next step is to calculate the expected value for the Allan variance from a set of m' independent measurements to obtain a more precise estimate for the detection limit. If s denotes the subensemble number, the ensemble average $\langle \rangle_e$ of the Allan variance $\langle \sigma_A^2 \rangle_e$ is given by:

$$\langle \sigma_A^2 \rangle_e = \frac{1}{2m'} \sum_{s=1}^{m'} (A_{2,s} - A_{1,s})^2, \quad (7)$$

$$A_{n,s} = \frac{1}{k} \sum_{l=1}^k x_{[(n-1)k+l],s}, \quad n = 1, 2.$$

From the expected values, the associated variances can be calculated and give a measure of the accuracy. If the system is ergodic the ensemble average $\langle \sigma_A^2 \rangle_e$ can be replaced by the time average $\langle \sigma_A^2 \rangle_t$ which is much more convenient for practical measurements [23] because sequential measurements are easier than simultaneous ones. As all averages and variances are a function of the subgroup ‘‘binsize’’ k , the time average $\langle \rangle_t$ of the Allan variance is then given by:

$$\langle \sigma_A^2(k) \rangle_t = \frac{1}{2m} \sum_{s=1}^m [A_{s+1}(k) - A_s(k)]^2$$

$$A_s(k) = \frac{1}{k} \sum_{l=1}^k x_{(s-1)k+l},$$

$$s = 1, \dots, m, \quad m = m' - 1. \quad (8)$$

$\langle \sigma_A^2(k) \rangle_t$ can be calculated by using the formulas derived above, and plotted against the averaging factor k on a log-log plot gives the ‘‘Allan-plot’’ [26] in Fig. 3. It is assumed that the data are collected over a constant time interval Δt , then the time $\tau = k \Delta t$ is equivalent to the averaging or integration time. The lower trace, with a minimum at an integration time of approximately 60-70 s, corresponds to the time-series data shown in Fig. 2a. The other trace of the Allan variance has been calculated from a data set containing a 10 times higher drift component.

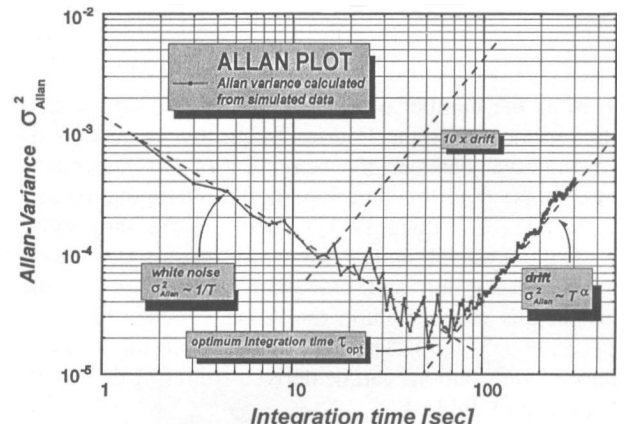


Fig. 3. ‘‘Allan-Plot’’ calculated from the data in Fig. 2a. At low integration times white noise dominates and σ_{Allan}^2 decreases proportional to the integration time. The drift influence begins to dominate beyond the optimum integration time τ_{opt} , $\alpha = 2$ describes the influence of a linear drift

The decreasing dashed line shows the theoretically expected behaviour of a drift-free system containing only white noise.

After this formal description of the Allan variance and its relation to the variance of the mean, we will briefly review and discuss some properties of the Allan variance as a measure of system stability in the next section.

2 Allan Variance, System Stability and Duty Cycle

The major factor influencing high-sensitivity measurements is the system stability. As mentioned before, the signal from a perfectly stable system could be averaged infinitely from a theoretical point of view. Infinite averaging should lead to extremely sensitive measurements, provided that limitations of the dynamic range of the system can be neglected. Unfortunately, real systems are stable only for a limited time, and then the question is how long can TDLAS signals be averaged to achieve an optimum sensitivity with a given spectrometer and application? It is obvious that every real unstable system will have an optimum averaging time given by the drifts in the system such as temperature drifts, moving fringes, changes in background spectra, etc. Consequently, the quality of the spectrometer is given by its stability which, in analogy to other stability investigations, can be described using the Allan variance [24,26,27], which has been derived in the last section. The Allan variance as a function of the integration time τ , is the time average of the sample variance of two adjacent averages $A_k(\tau)$ and $A_{k+1}(\tau)$ of time-series data.

Noise contributions $S(f)$, which are encountered in most systems, are frequency independent “white noise” and frequency dependent $1/f$ and $1/f^\alpha$, ($\alpha > 1$) noise. The latter noise encompasses a noise at very low frequencies which can be considered as drift. The time domain stability σ_{Allan}^2 can be derived from the frequency domain stability $S(f)$. The general formal solution of the translation among frequency stability measures has been derived by Cutler [23] in 1971 as:

$$\langle \sigma^2(M, T, \tau) \rangle = \frac{M}{M-1} \int_0^\infty df S(f) \times \frac{\sin^2(\pi f \tau)}{(\pi f \tau)^2} \left(1 - \frac{\sin^2(\pi r f \tau M)}{M^2 \sin^2(\pi r f \tau)} \right)^2, \quad (9)$$

where M is the number of data points used in obtaining a sample variance, f is the Fourier frequency variable, T is the time interval between the beginning of two successive measurements, τ is the duration of the averaging period, and $r = T/\tau$. The quantity T/τ describes the duty cycle (DC) of the system, and $r = 1$ means no dead time due to data sampling and processing. For $M = 2$ one obtains, in this nomenclature, the Allan variance [24], i.e. $\sigma^2(2, T, \tau) = \sigma_{\text{A}}^2(T, r)$. The time dependence of the three main noise contributions can be derived from (9); the results are displayed in Table 1.

Neglecting duty cycle effects for a first interpretation, i.e. assuming $r = 1$ and $T = \tau$, the Allan variance can be written in the following form as a time-domain approximation:

$$\sigma_{\text{A}}^2(\tau) = c_{\text{white noise}}(1/\tau) + c_{1/f} + \sum_{\alpha} c_{\text{drift}, \alpha} \tau^\alpha, \quad (10)$$

Table 1. Dependence of the Allan variance as a function of the integration time for a given spectral noise density, with a duty cycle of 1

Noise type	Spectral density $S(f)$	$\sigma_{\text{A}}^2(\tau)$
White	f^0	$k_0 \tau ^{-1}$
$1/f$	f^{-1}	k_1
Drift	f^{-2}	$k_2 \tau $
Drift (linear)	f^{-3}	$k_3 \tau ^2$

where α characterizes the type of system drift. In the case of a linear drift, $A_{n+1} - A_n = \text{const } \tau$, we have $\alpha = 2$. This means that, depending on the number of averages k , at short integration times τ within the white-noise dominated region, the Allan variance decreases (proportional to $1/\tau$) with increasing integration time. As the integration time increases, the Allan variance shifts from this region into a drift-dominated region where it again starts to increase (proportional to the measurement time T). It has been mentioned in the previous section that in the white-noise dominated region the square root of the Allan variance is proportional to the detection limit and, therefore, can be used to predict the detection limit of a given system as a function of the integration time. The Allan variance plotted as a function of the integration time leads to the Allan plot, as shown in Fig. 3. The minimum in the Allan variance corresponds to the optimum integration time τ_{opt} , indicated in Fig. 3. The optimum integration time is a characteristic property for a given instrument: it reflects the system stability (e.g. quality of line locking, drifts of fringes, changing background, etc.). Some important conclusions can be drawn from the Allan plot. The experimentally determined optimum integration time τ_{opt} represents the time τ_{meas} within which the sample and the background spectra have to be acquired:

$$\tau_{\text{opt}} > \tau_{\text{meas}}(\text{Background}) + \tau_{\text{exchange}} + \tau_{\text{meas}}(\text{Sample}) + \tau_{\text{exchange}} \quad (11)$$

where τ_{exchange} is the time required for the removal of ambient air from the absorption cell. For achieving the same signal-to-noise ratio the times for background and sample measurements should be set equal and therefore the actual optimum spectra measurement time is:

$$\tau_{\text{meas}} < (\tau_{\text{opt}} - 2 \tau_{\text{exchange}}) / 2 \quad (12)$$

If sample and background spectra are acquired subsequently and the integration times are chosen to be smaller or equal to τ_{meas} system drifts will not influence the quality of the data significantly. After this first drift correction the data can be stored again and analyzed in terms of the Allan variance to find the maximum possible system integration time. We used the Allan variance as a tool to characterize the overall stability of the spectrometer or of its individual components (current controller, temperature controller, etc.), and to determine the optimum integration time. An example of an experimental Allan variance analysis will be given in the next section.

As mentioned before, the drift-free part of the Allan plot is equivalent to the variance of the mean and its square root

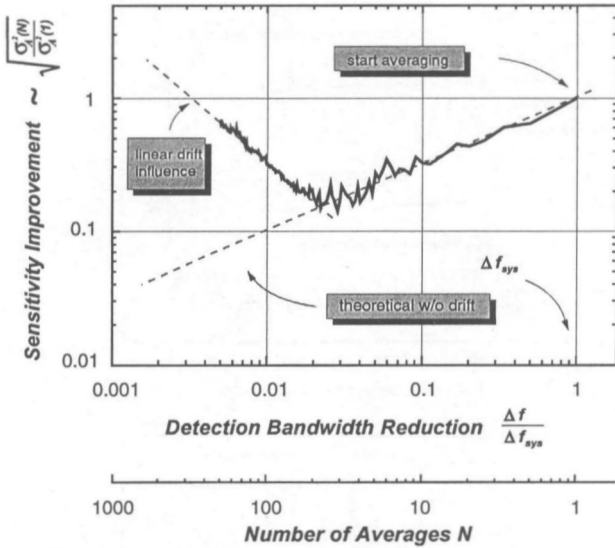


Fig. 4. The normalized Allan variance, which is proportional to the detection limit improvement, is plotted as a function of the electronic system bandwidth reduction. This plot can be used to predict the optimum number of averages and the detection limit for a given system and corresponds to the plot in Fig. 1

is a measure of the detection limit. While the integration time is inversely proportional to the detection bandwidth, a plot of the sensitivity improvement versus the effective system bandwidth Δf_{eff} can be derived from the Allan plot. Such a plot is shown in Fig. 4 and it can be seen that it is equivalent to the plot in Fig. 1. In Fig. 4 both axes are normalized, one to a single measurement and the other to the system bandwidth to indicate the improvement directly as a function of the number of averages. This shows that we can determine the optimum integration time, which is equivalent to the minimum achievable bandwidth, by analyzing system data in terms of the Allan variance and predict the detection limit of the investigated system.

So far, the analysis has been made under the assumption that there is no loss in measurement time due to the data acquisition. In most real systems, however, the loss in measurement time due to limited data transfer rates or extensive online data processing cannot be neglected. Consequently, it is interesting to investigate the influence of loss in measurement time. As before, T is the time between the beginning of successive measurements of duration τ . For a basic approach we do not use the equations in Table 1, but instead

$$\delta_A^2(\tau) = \sum_{\alpha} k_{drift,\alpha} T^{\alpha} + k_{1/f} + k_{white\ noise} 1/\tau \quad (13)$$

Using the duty cycle $DC = \tau/T$, the Allan variance can be plotted (Fig. 5) as a function of the measurement time T , or the integration time τ , parametrized by the duty cycle DC . The lowest trace in Fig. 5 represents an ideal system with a duty cycle of 100%. Due to the high duty cycle the signal-to-noise ratio improves rapidly (measurement time = integration time) and the line representing the system drift $k_{Drift} T^{\alpha}$ is reached after approximately 43 relative time units (A), in this example. The upper trace in Fig. 5, corresponds to a duty cycle of only 10% and starts to be

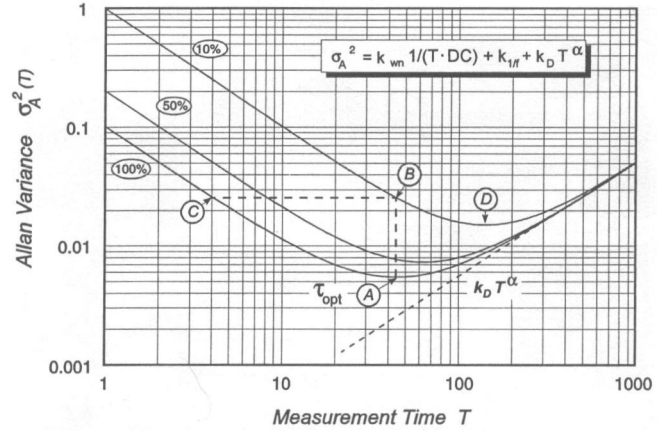


Fig. 5. Allan variance as a function of the measurement time for different duty cycles of 10%, 50%, and 100%; $DC = \tau/T$

drift influenced at about 140 relative time units (D), due to the less efficient use of the measurement time. The reduction of the white noise by averaging is much slower with a low duty cycle, and at substantially higher levels, the averaging process deteriorates, due to the drift component. When the 100% duty cycle system has reached its optimum integration time (A) and therefore its highest sensitivity, the 10% system has reached a detection level (B), which the 100% system has reached in about one tenth of the time (C).

This analysis shows that the duty cycle of the data-acquisition system should be as high as possible to achieve optimum system performance; note that only the duty cycle and not the overall data-acquisition rate influence the system performance. With respect to Fig. 5, the time scale could be in ms, s or even minutes. Data-acquisition systems based on a RS232 interface or IEEE-bus often substantially reduce the duty cycle of the spectra acquisition at high data-acquisition rates due to their limited data transfer speed and hand-shake procedures. To increase the duty cycle for spectra acquisition, it is recommended that parallel data processing using transputer technology and real-time digital signal processing be used. This is advantageous especially in multi component instruments where for each target gas the spectral data have to be averaged and analyzed parallel in real time to applications where a real-time display of concentrations is required.

3 Experimental Results

The performance of a single-tone frequency-modulated (FM) TDLAS instrument designed specifically for field measurements was analyzed in terms of the Allan variance introduced in the preceding sections. The measurements focussed on NO_2 one of the important atmospheric pollutants. The instrument was similar to that described by Werle [16] but the single-pass absorption cell was replaced by a multipass White cell.

The optical system of the instrument is shown schematically in Fig. 6. A diode laser (Fujitsu TDL-1600-N-OSI) is housed in a liquid-nitrogen cooled dewar. The laser light is collected and collimated by an off-axis paraboloid mirror

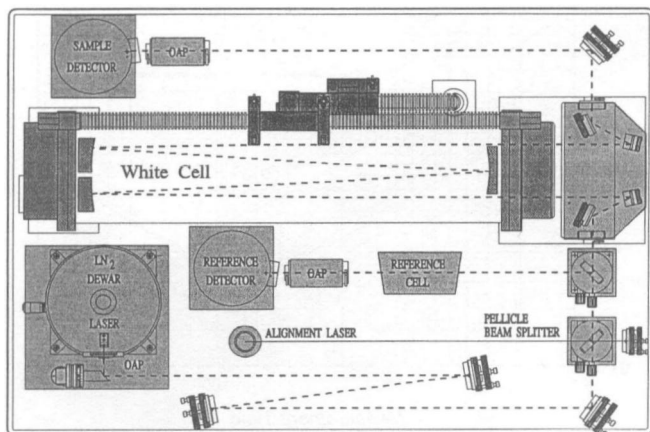


Fig. 6. Layout of the FM spectrometer for the detection of atmospheric trace gases

(OAP). The laser beam is then directed onto the entrance of a commercial White cell module (base length 62.5 cm, Müttek MDS 1600) with internal focusing optics. The outgoing beam is directed onto a high frequency HgCdTe photo-voltaic detector (Société Anonyme de Telecommunications, Model C1A). A beamsplitter in front of the White cell module directs part of the laser light through a reference absorption cell filled with NO, at a pressure of a few millibars and is detected by a second high-frequency HgCdTe detector. The signal from this reference channel is used to monitor the line shifts and to lock the laser frequency to the absorption line by adjusting the laser temperature or current. The optical setup can be prealigned using a 670 nm semiconductor laser coupled into the spectrometer path by a pellicle beam splitter. Because of low transmission in the infrared, the pellicle beam splitter is kinematically mounted and can be removed during the trace-gas measurements. To accommodate a possible deviation angle between the lobe of laser emission and the laser mount axis, the LN₂-dewar is mounted on a xyz-stage alignable within 30°. For optimum signal-to-noise ratio [28], the absorption path length in the White cell is adjusted to 27.5 m. The optical setup is mounted on a 1 m x 0.6 m optical breadboard and is enclosed in a box to improve the thermal stability and, by flushing the box with dry nitrogen, changing broadband atmospheric absorptions are reduced. The electronic setup for laser modulation and signal detection of the single-tone FM-TDLAS instrument has been reported by Werle et al. [9]. The frequency of the laser was swept over the selected NO₂ absorption line by a ramp from a computer controlled ramp generator. The sweeping frequency was chosen to be 345 Hz to discriminate against mechanical vibrations.

For the selection of an absorption line the laser could be tuned without mode hop from 250 mA to 290 mA and the FM spectrum was recorded with and without calibration gas. These records are shown in Fig. 7a together with a transmission signal from a Germanium etalon. After background subtraction the resulting spectrum was linearized using the Ge etalon fringe spacing to obtain the upper trace in Fig. 7b. For NO₂ measurements the absorption line at 1600.413 cm⁻¹ was chosen since its background was almost free of disturbance from the nearby pressure-broadened H₂O lines. The line consists of two unresolved lines of equal line strength of

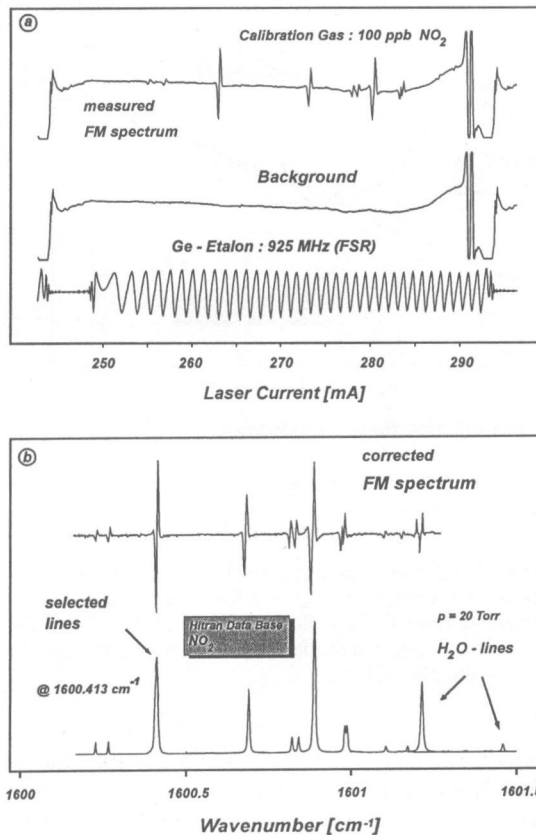


Fig. 7. a Recorded traces of calibration gas, zero air for background determination and Ge etalon for frequency linearisation. b Line identification: corrected FM spectrum of NO₂ vs HITRAN data

1.17×10^{-19} cm/molecule. The line identification was confirmed by comparing the FM spectra of NO₂ with water traces using the HITRAN line compilation [29] (Fig. 7b). The optical density of the 100 ppbv NO₂ calibration gas in a White cell was calculated to be 5.3‰ using a Voigt profile and was in good agreement with the direct absorption measurement with a photoconductive detector without frequency modulation. Consequently, 1 ppbv of NO₂ in the following data corresponds to an optical density of about 5×10^{-5} .

To characterize the performance of the instrument in terms of the NO₂ detection limit and detectable optical density, a series of NO₂ measurements in ambient air have been made. A characteristic FM spectrum obtained from an ambient raw spectrum after background subtraction is shown as the lowest trace in Fig. 8. This spectrum is the result of averaging 256 spectra in 740 ms and is almost noise free on this scale. The electronic bandwidth was set to 1.5 kHz. The spectra averaging then results in an effective bandwidth of 5.86 Hz. The mixing ratio of NO₂ was calculated by a least-squares fit of 27 channels to the corresponding channels of the calibration spectrum at 12 ppbv. The fit resulted in a mixing ratio of 1.17 ppbv with a 1σ error of 31.5 pptv. The confidence range given in Fig. 8 is defined as the fit-error times the Student t-factor at 95% statistical significance. Using 25 degrees of freedom in the fit, the t-factor is 2.06 leading to a confidence range of 63 pptv. The measured NO₂ FM-spectrum corresponds to an optical density of $62 \pm 3.34 \times 10^{-6}$ measured within 740 ms.

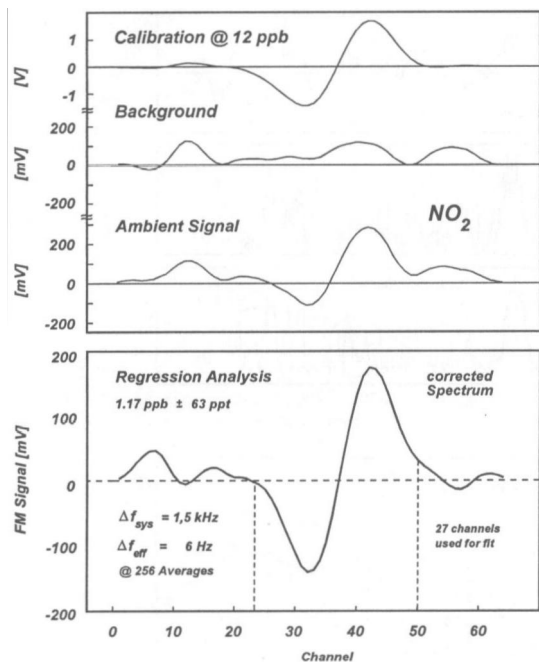


Fig. 8. FM signal of 1.17 ppb NO₂ in ambient air; spectra were averaged 256 times over 740 ms

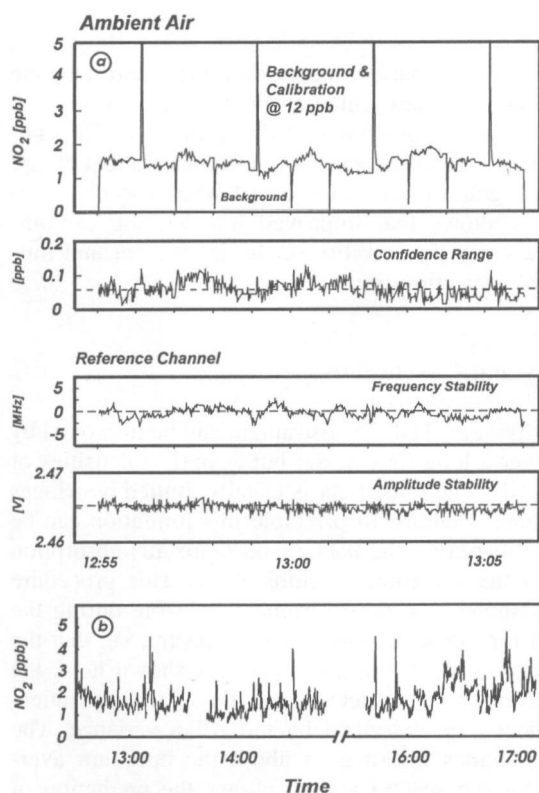


Fig. 9. a A record of NO₂ monitoring in ambient air using the FM instrument with a time resolution of 1.5 s. b total data set

Spectra like those in Fig. 8 were recorded for several hours. Figure 9b shows a continuous NO₂ measurement in ambient air. The data were obtained near the institute with a time resolution of 1.5 s (50% DC) during one afternoon. The observed NO₂ spikes are due to cars coming in and out of a

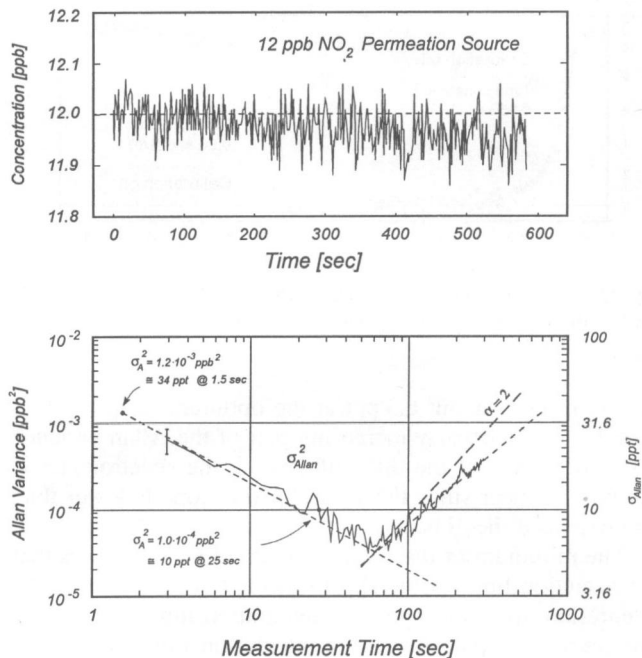


Fig. 10. Measurement of a 12 ppb NO₂ calibration gas mixture and the corresponding “Allan-Plot” as a function of integration time. The minimum indicates that the most sensitive measurements can be achieved with a 60 s integration time. As no drift should occur between background and sample measurement, the maximum available averaging time is 25 s, yielding a minimum of about 10 ppt

nearby parking lot, most of the regular spikes are coincident with the local bus schedule. The calibration and background measurements have been removed from the plot to avoid confusion. Figure 9a shows an expanded part of these data and the record of some control parameters for amplitude and frequency stability of the system. The presentation of NO₂ concentrations in the upper trace includes background and calibration measurements which have been omitted in Fig. 9b. For a complete description of the measurement, the frequency and amplitude stability of the reference channel are also shown in the lower two traces of Fig. 9a. The second trace shows the confidence range for each measured point with an average value of 65 pptv. The total confidence range varies from approximately 10-100 pptv. The system will be analyzed in detail to investigate the reason for this variation.

The performance of the system, characterized by the Allan variance, as proposed in the previous sections, has been investigated and the result is shown in Fig. 10. The Allan plot was generated from a continuous measurement of zero air spiked with 12 ppbv of NO₂ from a calibration source for a period of 600 s with a time resolution of 1.5 s. The linearly decreasing part of the Allan variance is white-noise dominated, and the value of the Allan variance in this part is equivalent to the value of the statistical variance. Consequently, the square root of σ_A^2 is an estimate of the detection limit. At an effective integration time of 1.5 s the detection limit estimated from the Allan variance (1.2×10^{-3} ppb²) was 34 ppt ($\pm 25\%$), which was in good agreement with the detection limit estimated from the fit errors (1a) at small concentrations (3.15 ppt). Further averaging of spectra improves the Allan variance to 4×10^{-5} ppb² giving a de-

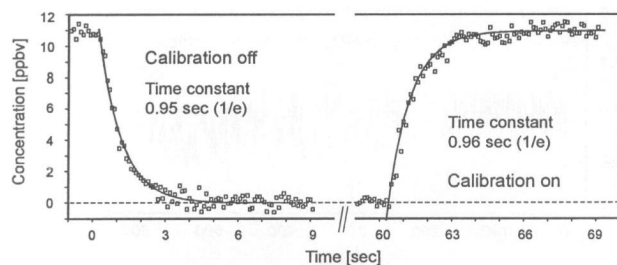


Fig. 11. Determination of the exchange time constant for the White cell used in the FM measurements, which is about 5 s for 99% removal

tection limit of about 6.3 ppt at the optimum integration of 60 s. From the linearly increasing part of the Allan variance it can be seen that the drift influencing the spectrometer is not purely linear since the value for the slope is lower than that expected theoretically.

The minimum of the Allan variance at 60 s indicates that the detection limit of the spectrometer can be improved by integration up to the optimum integration time τ_{opt} , 60 s in this particular case. At longer integration times, the Allan variance, and with it the instrument detection limit, will start to deteriorate as a consequence of instrumental drifts. In practical terms this means that the complete measurement sequence consisting of the acquisition of the ambient air, zero air and calibration gas spectra has to be completed within 60 s. For calibration purposes higher concentrations are usually used with correspondingly large signals that are much larger than the fringes in the FM spectrum. Provided that the laser frequency is kept constant by line locking, the acquisition of the calibration spectrum can then be omitted from the measurement sequence. This is advantageous since a substantial part of the time is needed to exchange the gas in the White cell after switching, say, from zero to ambient air. To investigate the time required for gas exchange in the multipath absorption cell, NO_2 calibration gas with a mixing ratio of 11 ppbv from a permeation source was switched off and on. During this experiment the flow through the White cell with a volume of about 6 l operated at 26.7 mbar was 10 l/min STP (0°C , 1013 mbar). The exchange time τ_{exchange} ($1/e$), calculated from the signal response in Fig. 11 was approximately 0.95 s. The exchange time to achieve 99% exchange is then approximately 5 s. Taking this gas exchange time into account, only 25 s are available to take each measurement and background spectra. Based on the achieved detection limit of 34 pptv at a 1.5 s measurement time, the spectra integration during this time interval would then improve the detection limit to about 10 pptv, corresponding to a detectable optical density of 5×10^{-7} . As it has been mentioned before, the duty cycle for these measurements was approximately 50%. At a 100% duty cycle, an improvement by a factor of $\sqrt{2}$ could be possible (Fig. 5), but this has not yet been demonstrated in practice because of the limiting data-processing capabilities.

Some factors controlling system stability were investigated by monitoring several parameters during the measurement. The analysis of these measurements revealed a good correlation between the deviation of line locking from the line center (in MHz) and the confidence range obtained from the fit. The upper trace of Fig. 12 shows the measured drift

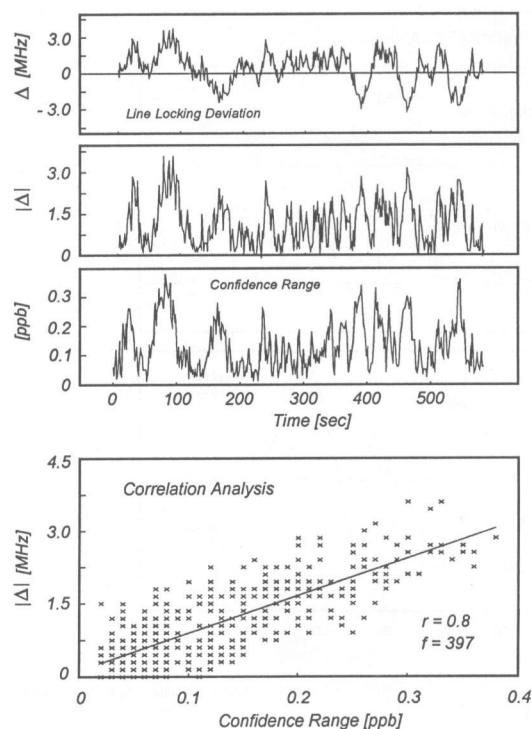


Fig. 12. Correlation analysis of layer stability and confidence range

of the line-locking deviation, the second trace represents the absolute deviation values which correlate well with the calculated confidence range shown in the third trace. The confidence range under 'line-locked' conditions is about 50 ppt and it may degrade by a factor of 10 when the deviation is large. This shows that improved line locking can improve substantially the stability of the instrument and thus the achievable detection limits.

4 Summary and Conclusions

The sensitivity of an TDLAS instrument can be improved by averaging over a long time scale; but at optical densities of the order of 10^{-6} the sensitivity is usually limited by fringes due to unwanted etalons. In principle this limitation can be avoided by subtracting the background (zero air) absorption spectra from the spectrum of ambient air. This procedure inherently assumes that the instrument is stable during the time needed for the acquisition of both spectra, i.e. that the fringes do not move in the meantime. As shown here, the stability and the resulting detection limits of the instrument can conveniently be described by the Allan variance. The Allan plot provides information about the optimum averaging time for the spectra and so allows the prediction of the ultimate detection limits of the spectrometer. The Allan variance can also be used to analyze the performance of individual components of the spectrometer. If the optimum integration time has already been determined for an instrument, it may be necessary to check its value from time to time, especially under field-operating conditions or in monitoring station systems, where parameters could change and so degrade the system's performance. With an automated spectrometer, the stability tests can be run under computer

control by analyzing a time series of low-level calibration data and, therefore, the system can be placed under adaptive control for the averaging time constant to collect background and ambient spectra.

A proposed use of the Allan variance has been demonstrated using an actual FM-TDLAS instrument with a multipass absorption cell. The detection limit of 31.5 pptv mixing ratio of NO₂ with an effective bandwidth of 5.86 Hz was in good agreement with the detection limit derived from the Allan variance (34 pptv). The analysis further indicated that the best detection limits can be obtained when the whole measuring sequence, consisting of the ambient and zero air spectra, is completed within the optimum integration time τ_{opt} which was 60 s in the case of our instrument. Taking this optimum integration time and the gas exchange in the multipass absorption cell into account, the detection limit could be improved to about 10 pptv, corresponding to a detectable optical density of 5×10^{-7} . Further improvements of the detection limit could be possible by improving the line-locking system, reducing cell volumes for faster gas exchange, and by raising the duty cycle for the spectra acquisition and averaging system.

If the first stage optimum integration time has been determined by the procedures described above, the ambient and the corresponding background spectra must be measured within this time to make sure that no significant drift degrades the system's performance.

This procedure should reduce significantly drift effects in the concentration values. From a theoretical point of view the observed drift effect should be eliminated but, practically, residual drifts will occur. It is important then that the resulting data are again analyzed in terms of the Allan variance. The expected minimum resulting from this second-stage Allan plot gives an estimate for the ultimate sensitivity which can be achieved.

Acknowledgements. This work was funded by the Bayerisches Staatsministerium für Wirtschaft und Verkehr and the German Ministerium für Forschung und Technologie (BMFT) as a contribution to the EUROTRAC subproject JETDLAG. We thank Prof. R. Schieder from the University of Cologne for valuable suggestions about the Allan variance.

References

1. C.R. Webster, R.T. Menzies, E.D. Hinkley: In: *Laser Remote Chemical Analysis*, ed. by R.M. Measures (Wiley, New York 1988) p. 163
2. B.J. Finlayson-Pitts, J.N. Pitts, Jr.: *Atmospheric Chemistry* (Wiley, New York 1986) p. 326
3. R. Grisar, H. Böttner, M. Tacke, G. Restelli (eds.): *Monitoring of Gaseous Pollutants by Tunable Diode Lasers* (Kluwer, Dordrecht 1992)
4. D.R. Hastie, G.I. Mackay, T. Iguchi, B.A. Ridley, H.I. Schiff: *Environ. Sci. Technol.* 17, 352A (1983)
5. H.I. Schiff, G.W. Harris, G.I. Mackay: In: *The Chemistry of Acid Rain*, ed. by R.W. Johnson, G.E. Gordon, W. Calkins, A.Z. Elzerman (Am. Chem. Soc., Washington 1987) p. 274
6. P. Wameck: *Chemistry of the Natural Atmosphere* (Academic, London 1988)
7. D.R. Crosley, J.M. Hoell (eds.): *Future Directions for H_xO_y detection* (NASA Conference Publication No. 2448, Washington 1986)
8. G.C. Bjorklund: *Opt. Lett.* 5, 15 (1980)
9. P. Werle, F. Slemr, M. Gehrtz, Chr. Bräuchle: *Appl. Phys.* B49, 99 (1989)
10. J.A. Silver: *Appl. Opt.* 31, 707 (1992)
11. D.S. Bomse, A.C. Stanton, J.A. Silver: *Appl. Opt.* 31, 718 (1992)
12. C.R. Webster: *J. Opt. Soc. Am.* B2, 1464 (1985)
13. J.A. Silver, A.C. Stanton: *Appl. Opt.* 27, 4438 (1988)
14. J. Reid, M. El-Sherbiny, B.K. Garside, E.A. Ballik: *Appl. Opt.* 19, 3349 (1980)
15. C.B. Carlisle, D.E. Cooper: *Opt. Lett.* 14, 1306 (1989)
16. F. Slemr, G.W. Harris, D.R. Hastie, G.I. Mackay, H.I. Schiff: *J. Geophys. Res.* 91, 5371 (1986)
17. G.W. Harris, G.I. Mackay, T. Iguchi, H.I. Schiff: *J. Atmos. Environ.* 8, 119 (1989)
18. F.C. Fehsenfeld, J.W. Drummond, U.K. Roychowdhury, P.S. Galvin, E.J. Williams, M.P. Buhr, D.D. Parrish, G. Hübler, A.O. Langford, J.G. Calvert, B.A. Ridley, F. Grahek, B.G. Heikes, G.L. Kok, J.D. Shetter, J.G. Walega, C.M. Elsworth, R.B. Norton, D.W. Fahey, P.C. Murphy, C. Hovnermale, V.A. Mohnen, K.L. Demerjian, G.I. Mackay, H.I. Schiff: *J. Geophys. Res.* 95, 3579 (1990)
19. J.K. Taylor: *Quality Assurance of Chemical Measurements* (Lewis, Chelsea 1988) Chap. 14
20. R.O. Gilbert: *Statistical Methods for Environmental Pollution Monitoring* (van Nostrand Reinhold, New York 1987) Chap. 15
21. I.N. Bronstein, K.A. Semendjajew: *Taschenbuch der Mathematik*, 19th edn. (Teubner, Leipzig 1979) Chap. 5.2
22. L. Sachs: *Angewandte Statistik*, 5th edn. (Springer, Berlin, Heidelberg 1978)
23. J.A. Barnes, A.R. Chi, L.S. Cutler, D.J. Healey, D.B. Leeson, T.E. McGunigal, J.A. Mullen, W.L. Smith, R.L. Sydnor, R.F.C. Vessot, G.M.R. Winkler: *IEEE Trans. IM-20*, 105 (1971)
24. D.W. Allan: *Proc. IEEE* 54, 221 (1966)
25. J.A. Barnes: NBS, Washington, DC. Tech. note 375 (1969)
26. W. Demtröder: *Laser Spectroscopy* (Springer, Berlin, Heidelberg, 1982) p. 225
27. R. Schieder, G. Rau, B. Vowinkel: *Proc. SPIE* 598, 189 (1985)
28. P. Werle, F. Slemr: *Appl. Opt.* 30, 430 (1991)
29. HITRAN: L.S. Rothman, R.R. Gamache, A. Goldman, L.R. Brown, R.A. Toth, H.M. Pickett, R.L. Poynter, J.-M. Flaud, C. Camy-Peyret, A. Barbe, N. Husson, C.P. Rinsland, M.A.H. Smith: *Appl. Opt.* 26, 4058 (1987)